



Revolutionizing prostate cancer diagnosis: Unleashing the potential of an optimized deep belief network for accurate Gleason grading in histological images



S. Angel Latha Mary^{a,*}, S. Siva Subramanian^b, G. Priyanka^c, T. Vijayakumar^d, Suganthi Alagumalai^e

^a IT Department, SNS College of Technology, Coimbatore, India

^b Department of BME, Rathinam Technical Campus, Coimbatore, India

^c Department of Computer Science and Business Systems, Sri Eshwar College of Engineering, Coimbatore, India

^d Department of AIDS, Dr.Mahalingam College of Engineering and Technology, Pollachi, Coimbatore, India

^e Cyber Operations, 3223 Hanover St, Palo Alto, CA, 94304, USA

ARTICLE INFO

Keywords:

Prostate cancer
Gleason grading
Histological images
Elephant herding optimization
Hyper-parameter and Gaussian kernels

ABSTRACT

PC (Prostate Cancer) is the second highest cause of death due to cancer in men globally. Proper detection and treatment are critical for halting or controlling the growth and spread of cancer cells within the human organism. However, evaluating these sorts of images is difficult and time-consuming, requiring histopathological image recognition as the most reliable method for treating PC because of its distinct visual characteristics. Risk evaluation and treatment planning rely heavily on histological image-based Gleason grading of prostate tumors. This work introduces an innovative approach to histological image analysis for prostate cancer diagnosis and Gleason grading. The Elephant Herding Optimization-based Hyper-parameter Convolutional Deep Belief Network (CDBN-EHO) is presented alongside a grading network head-optimized deep belief network technique for multi-task prediction. Leveraging an effective Bayesian inference method, fully linked Conditional Random Field (CRF) techniques are utilized for segmentation, with pairwise boundary capacities determined by a linear mixture of Gaussian kernels. The multi-task approach aims to enhance performance by incorporating contextual information, leading to breakthrough results in the identification of epithelial cells and the grading of Gleason scores. The objective of this study is to demonstrate the effectiveness of the optimized deep belief network technique in improving diagnostic accuracy and efficiency for prostate cancer diagnosis and Gleason grading in histological images.

1. Introduction

In India, PC ranks among the top 10 most common malignancies. Men over the age of 65 are most likely to be affected by this condition. However, there has been an increase in the number of cases of cancer reported in younger men living in urban areas who are between the ages of 35 and 44 and between 55 and 64 in recent years. Some of the most significant factors that have been found to increase the risk of prostate cancer are becoming older, being overweight, eating an unhealthy diet, and having genetic changes. Cancer has a 64 % cure rate after 5 years in patients in India. According to the findings of a study that was carried out in Mumbai, patients who received PC treatment that also included

surgery had a higher chance of surviving the disease (91 %). These findings demonstrate that despite the fact that therapy has the potential to save a life or increase the number of years a person can live, it is more important than ever to raise awareness about the disease and take steps to prevent it. Estimates of the number of people diagnosed with PC in India for the years 2010 and 2015 were respectively 26,120 and 28,079 [1]. The number of new instances of this disease is expected to more than quadruple by the year 2020, according to the data that was gathered from cancer projections. Incidence rates of this type of cancer are consistently and rapidly increasing.

Artificial Intelligence (AI) methods are computer algorithms that learn patterns from previously collected data in order to qualify

* Corresponding author.

E-mail addresses: xavierangellatha@gmail.com (S. Angel Latha Mary), siva.ace@gmail.com (S. Siva Subramanian), priyanka.gcse@sece.ac.in (G. Priyanka), vijayakumart@drmcet.ac.in (T. Vijayakumar), Suganthi.Alagumalai@JPMChase.com (S. Alagumalai).

predictions in novel data that has not been seen. Earlier iterations of AI made use of what are now commonly referred to as ‘conventional’ machine learning (ML) methodologies. These procedures were frequently carried out in two stages. To begin, domain experts (humans who are specialists in the subject area) painstakingly created features to excerpt numerical characteristics from the data that were particular to the task at hand. For instance, tumor size or form was one of the variables that was extracted. Second, these manually produced features were input into automated detection techniques in order to discover which aspects were helpful and how to integrate them in order to achieve the highest level of accuracy possible when classifying data into categories (for example, benign nodules versus malignant tumors). These AI methods can be trained to make predictions based on data they have never seen before, and then utilized to make predictions in novel contexts. Deep learning (DL) approaches were made possible by recent advances in the computational capability of graphics processing units, commonly referred to as GPUs. Because deep learning techniques eliminate the requirement for hand-crafted features, they can function in a completely computerized manner to not only detect the characteristics but also use them for the task that is wanted further down the line. DL techniques have brought about a sea change in the field of AI as a result of their exceptional performance, which frequently exceeds that of humans, notably in activities linked to image processing.

The field of medical imaging, especially detection using automated assessment, which is the incorporation of imaging function architecture based on machine learning, has shown that it can help radiologists make correct diagnoses, which cuts down on diagnostic time and also screening costs. The USG (Ultra Sono-Grphy) technique is a sort of imaging technology used in the first detection step and is based on real-time images. This method, however, cannot yield the best outcomes due to the absence of contrast between cancer and benign tissue [2]. Despite its lack of real-time imaging capability, mpMRI (multi-parametric magnetic resonance imaging) tends to be more precise than ultrasound due to superior tissue contrast. However, in order to use it, extensive training is necessary [3].

The areas of the skull and neck, cervical, and pelvic cavity can all be treated with brachytherapy, which is a form of radiation therapy. With this method, the radioactive beam is aimed directly at the area of the body that has been damaged. There are two different approaches to brachytherapy: permanent installation, which is also referred to as seed placement, and removal of radioactive material [4]. It has been found that brachytherapy, which involves the use of seeds, is more real in treating prostate cancer than radical prostatectomy. In a procedure called brachytherapy, which is used to operate on the prostate, pellets, which are little seeds, are positioned on the prostate cell. These pellets are quite small but contain radioactive materials. This highly radioactive substance is toxic to PC cells and destroys them. It is possible that this will cause destruction or even death to the strong cells that are located close to the prostate as a side effect.

The results of applying DL strategies to various applications, such as object identification, segmentation, and classification, have been encouraging. These methods involve the use of convolution layers, each of which is able to excerpt a unique set of features from the input photographs by using local low-level features as a starting point and working their way up to global high-level features. At the boundary of the coevolutionary neural layers, a fully linked layer transforms complicated features in terms of signal likelihood [5,6]. The batch normalization layer, which adjusts the provided input layer with zero means, and the unit variant with a dropout layer, which appears to be one of them of the normalization methods that disregard the nodes that are chosen in a randomly directed fashion, have each been given as various methods with which to enhance the output based on a DL-based technique. With these two layers, the output has been enhanced. However, in order to attain convincing efficiency, the appropriate combinations and layer topologies, along with appropriate fine-tuning of the hyper-parameters, are required. The following architecture, which is

illustrated in Fig. 1 and the key contribution of this work.

- To introduce a novel CDBN-EHO and a specialized deep belief network technique tailored for multi-task prediction, particularly in the context of segmentation tasks.
- This work also presents an advanced Bayesian inference method applied to fully linked CRF techniques for segmentation, where pairwise boundary capacities are determined using a linear mixture of Gaussian kernels.
- By adopting a multi-task learning approach, the proposed techniques aim to enhance performance by leveraging shared contextual information across tasks. Notably, these methods have achieved remarkable breakthroughs in the simultaneous identification of epithelial cells and grading of Gleason scores.

Overall, the combination of these techniques represents a significant advancement in the field of machine learning, particularly in the domains of multi-task prediction, segmentation, and grading. The demonstrated breakthrough results underscore the effectiveness and potential applicability of the proposed methodologies in various real-world scenarios.

The remaining of the paper is structured as follows: the related work PC using DL is discussed in section 2. The proposed methodology is explained in section 2 and the experimental results and analysis is explained in section 4. The final conclusion and future work are given in section 5.

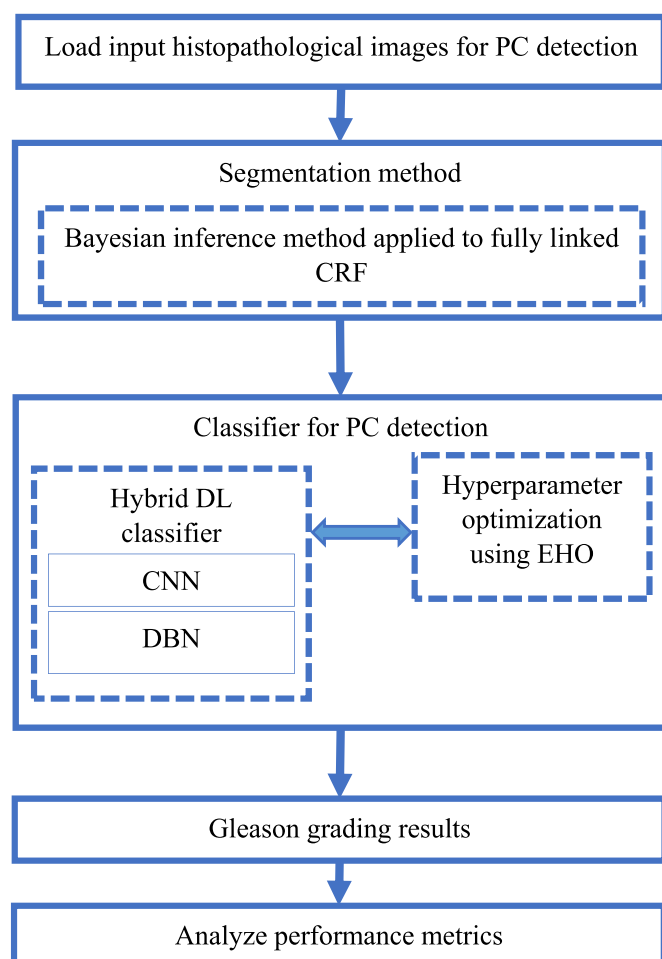


Fig. 1. Architecture diagram of Proposed Methodology for PC detection.

2. Related work

The LSTM (long short-term memory) and Residual Net (ResNet - 101) were used by Iqbal et al. [7], and both were trained without the use of any manually-created features and were then fine-tuned. Results from non-DL classifiers like the Gaussian Kernel, SVM (support vector machine), kernel naive Bayes, KNN - Cosine (k-nearest neighbor-Cosine), decision tree (DT), and RUSBoost tree were compared to features that were created by humans. Non-DL techniques with GLCM features utilizing KNN-Cosine achieved the best results, with 98.01 % sensitivity, 99.25 % specificity, 98.99 % PPV, 99.11 % NPV, 99.07 % accuracy, and 0.998 AUC. With DL method ResNet - 101, received (100 %) Accuracy and AUC (1) for Kernel Naive Bayes, RUSBoost Tree, and SVM Gaussian, whereas DL method LSTM produces performance with specificity (100 %), sensitivity (98.33 %), NPV (99.26 %), PPV (100 %), MCC (0.9879), accuracy (99.48 %), and AUC (0.9999).

Researchers Li et al. For PC pathological images, Furthermore presented a DL-based method for automatically determining the Gleason grading and segmenting the Gleason outline region. To ensure precise Gleason grading, Furthermore present an architecture for segmenting the Gleason pattern region that combines atrous spatial pyramid pooling with multiscale typical convolution. In addition, the prediction undergoes a post-processing approach employing conditional random fields. For the area covered by the Gleason pattern, the average%age of correct intersections over unions is 77.29 %, and the overall pixel accuracy is 89.51 %. In addition, the automatic Gleason grading yielded results that were on par with those obtained by human pathologists. Cohen's quadratic kappa revealed an average inter-annotator agreement among the technique and the pathologists of 0.77. The proposed research demonstrates that merging various DNN (Deep Neural Network) architectures is an effective strategy for producing more detached and predictable Gleason grading of PC.

Karimi et al. [9] proposed using a DL-based method of classification and data augmentation methods and accurate grading of PCa in histopathology images. The proposed method integrates the outputs of three independent CNNs (Convolutional Neural Networks) that are trained on progressively smaller patches. A logistic regression technique, trained independently of the CNNs, is then used to combine the predictions from the three CNNs. Then propose new data augmentation strategies and conduct empirical research into their influence on the classification accuracy to better train This algorithms. The suggested technique correctly identifies 92 % of malignant patches as cancerous rather than benign, and correctly 86 % of low-grade cancers.

An innovative DL-based CADS was presented by Duran-Lopez et al., [10]. After being patch-sampled and pre-processed with several filters, including a revolutionary patch-scoring method that gets rid of unimportant parts of the tissue, this system can interpret whole-slide histology images. The consequence that using a stain-normalization technique on the patches to lessen color variation between scanners is also analyzed. Utilizing 3-fold cross-validation for training, the network achieves 0.999 AUC, 0.999 F1 score, and 99.98 % accuracy on a new test set. The average processing time for generating a heatmap of an entire slide is 15 s. For a binary classification job between normal and cancerous prostate whole-slide images, This proprietary network beats prevailing advanced research in terms of computational complexity at the patch level.

Using a deep residual CNN, Kott et al. [11] were able to classify each patch on two different levels: (1) broadly (benign vs. malignant) and (2) specifically (benign vs. Gleason 3 vs. 4 vs. 5). Furthermore used five-sample cross-validation to assess the quality of This techniques. Hypothesis testing comparing actual technique performance with that expected by chance was conducted using randomization tests. Fine-grained classification of image patches as benign or malignant showed 91.5 % accuracy (p 0.001) using the technique (0.90 specificity, 0.93 sensitivity, and 0.95 average precision). The requirement for external validation and the relatively modest size of the sample are two

Table 1

The research gap of existing methods with advantages and disadvantages.

Author	Methods	Advantages	Disadvantages
Iqbal et al. [7],	LSTM-ResNet-101	Due to the contrast between malignant and benign tissue, these procedures can yield ideal results.	It cannot detect prostate cancers in other areas.
Li et al. [8],	Deep Neural Network	Reproducibility is restricted and can be applied fast in medical systems.	This method had obtained good results, but it required precise localization of small image portions in order to extract features.
Karimi et al. [9],	CNN	This approach could have reduced unpredictability in the production of large numbers of slides and increased their efficiency.	However, developing this approach is not a straightforward task because significant volumes of labeled training data are necessary.
Duran-Lopez et al. [10],	CNN	<ul style="list-style-type: none"> • By reducing the amount of data sampled during the generation and classification phases, this technique is able to speed up the learning and inference processes. • The use of a digital pathology image to enhance the CNN's adaptation for classification tasks. 	With a CNN-based setup, the computational cost of anticipating an input image is significantly higher, resulting in a longer processing time.
Kott et al. [11],	CNN	The sensitivity and specificity of this approach were both improved when applied to cancers.	However, their effect is diminished due to difficulties in reproducing and validating their findings.
Busby et al. [12],	SNN	Higher representation capacity describes this approach. Statistically, the effect of underperformance on other data was substantial.	Results were greatly exaggerated, and their significance was missed.
Ahmad et al. [13],	CNN	<ul style="list-style-type: none"> • However, present studies cannot answer if a PC symptom arises on any portion of the body. • This approach delivers adequate accuracy but necessitates clean, asymmetric, and sizable training datasets. 	
Swiderska-Chadaj et al. [14],	GAN	<ul style="list-style-type: none"> • This strategy has a greater chance of success. • The data produced by GANs resembles the original data quite closely and can be readily interpreted into variants. 	Continuously providing varied image data is required for testing purposes.
Kumar et al. [15],	VGGnet	This technique allows for precise remote prediction at a low cost and with lightning-fast comprehension.	High cost in carrying out the modifications; yet, the significance and relevance were not completely examined because of a lack of comprehensive.
Chatrian et al. [16],	DNN	Highly substantial changes in the forecasting of overall survival when	<ul style="list-style-type: none"> • But pathologic complete response rates were not

(continued on next page)

Table 1 (continued)

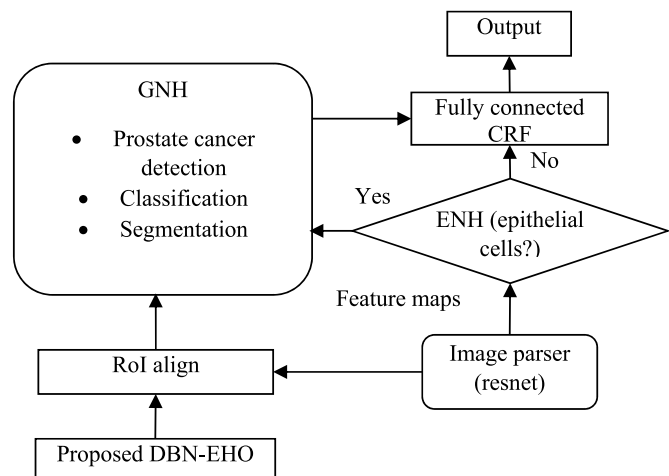
Author	Methods	Advantages	Disadvantages
		using this approach to determine the prostate size.	<ul style="list-style-type: none"> • Significantly different. • Poor contrast between hard and soft tissues.

limitations. Heterotopic choriocarcinoma was successfully diagnosed and graded using a DL-based computer vision algorithm in this study.

According to Busby et al. Shortages in the available workforce and inconsistencies in histopathological evaluation. These techniques, which include histopathological information into complex neural networks, perform exceptionally well at identifying, grading, and predicting outcomes for PC. In spite of the fact that fully autonomous PC diagnosis is still years away, new research indicates that AI is already being used as a preliminary screening tool, a companion in the form of a real-time interactive screen during histological analysis, and an additional read system to identify false negative diagnoses. The persistence of this work is to discuss the current state of AI in PC histopathology as well as its potential future applications.

Histopathologic images of lymph node sections were used by Ahmad et al. [13], to present a CNN-based technique for the categorization and diagnosis of metastatic cancer. The process of diagnosing cancer from histopathologic images is laborious and time-consuming for pathologists because a broad tissue area must be investigated, and even a single microscopic metastasis can be missed. Furthermore, took the required precautions against overfitting and improved the findings by doing the appropriate pre-processing and data augmentation activities. The method achieves excellent accuracy in cancer diagnosis through the use of low-dimensional representations and automated, specific feature extraction and classification. The experimental results for the medical image categorization and detection challenge demonstrate promising performance, with an accuracy rate of 0.94.

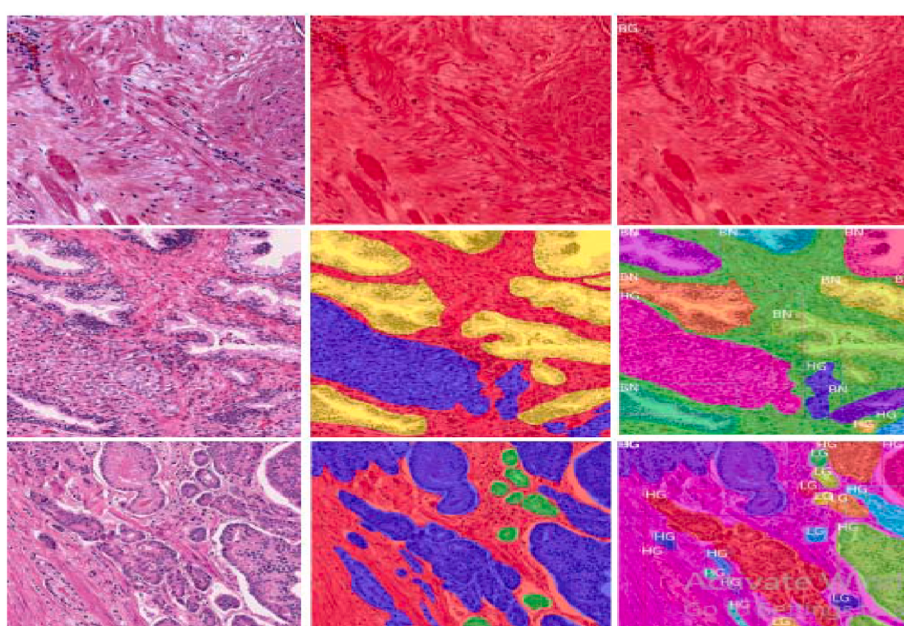
Swiderska-Chadaj et al. [14] analyzed the impact of imaging devices and cycle-GAN-based standardization on the efficacy of algorithms and evaluated several DL techniques for discovering PC in whole-slide images. Among the many networks tested in this work are U-Net, DenseNet, and EfficientNet. As a pre-processing phase, furthermore investigated the cycle-GAN-based normalizing technique and the WSICS

**Fig. 3.** Outline of the CDBN-EHO technique proposed architecture.

(whole-slide image color standardizer) technique. Furthermore, found an AUC of 0.92 and 0.83 for the two data sets that were treated separately. The AUC increases from 0.91 to 0.88 when rescanning, and from 0.97 to 0.98 when normalizing for formatting. This system may one day be implemented to mechanically pre-screen prostate biopsies, relieving pathologists of some of their duties.

According to Kumar et al. Using differential privacy and safe multi-party computation, a robust framework was proposed for cancer diagnostic picture classification. Instead of doing the entire operation in the cloud, one can split the layers apart into two distinct modules: a single for feature extraction using the VGGNet module on the user side, and the other modules for private prediction in the cloud. Two data sets made up of histological images of canine mammary tumors and human breast cancer are used to verify the framework's efficiency. When applied to the suggested technique, differential privacy preservation makes it secure and able to protect private information from prying eyes without sacrificing performance. The suggested approach efficiently strikes a balance between privacy and technique performance, as demonstrated by a battery of experiments.

In a recent study, Chatrian et al. [16] showed how variational

**Fig. 2.** Original, benchmark, and problem-defining sample images.

autoencoders and generative adversarial networks may be used together to generate realistic histological images that can be used to train semantic segmentation techniques. Then examine if these techniques can be employed to separate out groups of prostate glands that share a common molecular signature. If this progress continues, it will lead to the identification of previously unknown histology-based subgroups of diseases. It shows that the expression of a clinical indicator in prostate glands can be identified using only morphological parameters extracted from H&E images.

Summary: Various studies have tackled prostate cancer diagnosis and Gleason grading using a range of techniques, including non-deep learning (DL) methods like Gaussian Kernel, SVM, and DL methods such as ResNet-101, LSTM, and CNNs. While non-DL techniques like GLCM features achieved high sensitivity and specificity, DL methods like LSTM demonstrated excellent performance with high accuracy and AUC shown in Table 1. Innovations in DL-based approaches, such as integrating CNNs and employing novel architectures, have led to significant advancements in automated Gleason grading and histological image interpretation. Despite the progress, challenges remain, including the need for further validation and addressing computational complexity. Nonetheless, AI applications show promise as screening tools and companions to pathologists, indicating a potential future for AI-assisted prostate cancer diagnosis. Traditional deep learning methods like CNNs, LSTM, and GAN have played crucial roles in image analysis tasks like classification and segmentation. However, they may fall short in fully leveraging contextual cues or handling multi-task prediction challenges, particularly in histological image analysis. Also, their computational complexity may hinder their efficacy, especially in addressing the intricacies of multi-task prediction, notably in histological image analysis. In contrast, the proposed method introduces innovative optimization techniques, such as EHO and hyper-parameter optimization, specifically tailored for multi-task prediction. Moreover, optimizing the DL architecture for grading tasks reflects a targeted strategy for addressing the intricacies of Gleason grading in histological images. Through an emphasis on multi-task learning and task-specific optimizations, the proposed method aims to elevate the performance of deep learning models in histological image analysis, potentially enhancing diagnostic accuracy and aiding clinical decision-making in fields like prostate cancer diagnosis.

3. Proposed work

As a means of addressing the issue raised in the introduction, this part provides an in-depth analysis of the unique CDBN-EHO framework. Finally, furthermore present the assessment metrics that were used to evaluate the proposed technique and compare it to prior attempts. Automation of tasks such as Gleason grading through advanced deep learning techniques can alleviate the burden on pathologists, who typically face heavy workloads and time constraints. By streamlining the analysis process, this method allows pathologists to focus their expertise

on more complex cases and critical decision points.

3.1. Dataset description

Grading histological images for Gleason scores is a challenging and time-consuming process that demands expertise and experience from pathologists. However, the development of automated methods offers a promising solution. These advanced techniques have the potential to accurately analyze histological images, providing valuable assistance to pathologists in their diagnostic workflow. By automating this task, workload can be reduced, and consistency in grading can be improved, ultimately benefiting both pathologists and patients. IRB number Pro00029960 authorizes the use of 513 images from the Pathology Department archives at Cedars-Sinai Medical Center as the basis for the proposed dataset. The 513 images are a mosaic made up of two different kinds of tiles. Twenty-four photos (Set A) from these individuals have been classified as having either stroma (ST), benign or normal glands (BN, scored as GG2 or lower), LG cancer (low-grade), or HG cancer (high-grade) [17]. The remaining 289 images come from 20 patients and depict various types of dense high-grade tumors, including both cribriform and non-cribriform glands with Gleason grades 5 (GG5) and 4 (GG4). Set B of these photos (included in Ref. [18]) consists entirely of stromal components including nerve tissue and blood arteries. Set A slides were scanned using a high-resolution whole-slide scanner SCN400F (Leica Biosystems, Buffalo Grove, IL), and Set B slides were scanned using the Aperio scanning system (Aperio ePathology Solutions, Vista, CA). Both systems used a 20 \times scanning objective. The final product was a color RGB image with an 8-bit intensity depth per color network and a pixel extent of 0.5 m 0.5 m. Whole Slide Images (WSIs) were partitioned into 1200 \times 1200-pixel tiles after representative tiles were manually selected by a pathologist. An experienced research pathologist used a custom-built graphical user interface to manually annotate the data included in each tile. Three samples from the dataset utilized in this work are displayed in Fig. 2. The pathologists checked each other's work and agreed on how to fix any discrepancies they found in the annotated image tiles. To accommodate for stain variation, all tiles had been normalized before further analysis. Images on the tiles were flipped, mirrored, and rotated before being transmitted into the network as a form of data augmentation. Both [17,18] make use of these same datasets from prior research. Please see the Supplementary Information for a detailed explanation of the Gleason grading system and the rationale for the choice to divide tissues into four groups.

i. Network architecture

Fig. 3 depicts the full system along with the individual parts of the suggested technique. For This proposed picture parser, furthermore rely on ResNet as the main neural network. The picture parser begins by creating feature maps. Two subsystems receive these feature maps as input. Similar to the CDBN-EHO, here used a two-stage process in the left

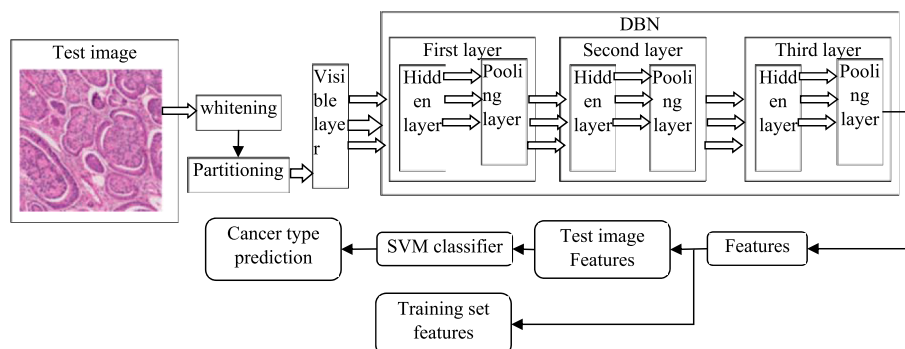


Fig. 4. The entire procedure of the proposed CDBN

fork. First, a RPN (Region Proposal Network) uses the feature maps to propose RoIs (regions of interest). To predict the box offset, class, and binary mask for each ROI, a GNH (Grading Network Head) is employed in the second step. Furthermore, augment this with a right fork that provides a score for the presence of epithelial cells in the image. The ENH (Epithelial Network Head) designates this section. Both the ENH and GNH results contribute to the final forecast generated by the network. The prediction is then subjected to a final round of processing in the form of a conditional random field.

ii. Objective function of CDBN-EHO

The suggested CDBN-EHO technique has two main functions: to identify epithelial cells and to generate a segmentation mask based on the Gleason score. The CD (Contrastive Divergence) and PCD (Persistent CD) are used to learn the weight matrix and corresponding bias vectors of the exposed and concealed nodes. Here, the BP is combined with a standard gradient ascent technique to find the best possible settings for the weight matrices. In order to reduce certain error metrics, the optimization process takes into account the results of an additional layer constructed on top of the DBN following its first greedy training. Logistic units also known as softmax are commonly utilized in this tier.

3.2. Convolutional deep belief network (CDBN)

The input images are processed using a whitening technique that removes the correlation between neighboring intensity levels. The process of whiten projection involves projecting the input image into the eigenvectors and normalizing them so that all intensity values have a variance of 1. The image that has been brightened is then specified to the visible layer of the CDBN, where it is separated at random into tiny batches that overlap with each other. Mini batches break up the input image into manageable pieces before applying the learning algorithm to each one. When the data sample is not representative of the total, these techniques reduce the amount of noise in the analysis. By utilizing a hierarchical framework, the CDBN technique is able to separate the low-level properties from the high-level ones. The Convolutional Restricted Boltzmann Machines (CDBMs) are generative techniques built from CRBMs stacked one on top of the other. As can be seen in Fig. 4, each CRBN has a hidden layer (\mathbb{H}), a visible layer (\mathbb{V}), and a pooling layer.

A $N_{\mathbb{V}} \times N_{\mathbb{H}}$ array of binary units makes up the viewable layer of the image. There is a total of $k \times N_{\mathbb{H}}^2$ hidden units since the \mathbb{H} is composed of k groups (also known as “bases”), each of which is an array of binary units with the dimensions $N_{\mathbb{H}} \times N_{\mathbb{H}}$. In the visible layer, there is a convolutional window with the dimensions $N_w \times N_w$ (where $N_w = N_{\mathbb{V}} - \frac{N_{\mathbb{H}}}{N_{\mathbb{H}}} + 1$), which is dedicated to each individual group. A weight matrix, denoted by the letter \mathbb{W} , is used to describe the symmetric relationships that exist between hidden and visible units. Here might think of each weight matrix as a filter if this method wanted to. In addition, there are k groups of units that make up the pooling layer, and inside each group, there are $N_p \times N_p$ binary units. A predetermined constant factor C is used by the pooling layer to reduce the size of the representation of the \mathbb{H} . In order to accomplish this goal, the pooling layer picks the values that are the highest in the $C \times C$ windows of the concealed layer. The use of maximum pooling not only makes it possible for the outputs of higher layers to remain invariant to changes of a more minute magnitude in the input, nonetheless it also lowers the overall computing cost. In order to extract features from histological images of neuroblastoma, furthermore make use of a CDBN with three layers. The CDBN that has been presented has some free parameters that still need to be established. The first factor to consider is the total number of concealed layers. While a CDBN with less \mathbb{H} s requires less time to train, its performance suffers as a result of the network's inability to ignore low-level details in the input images. The performance can be improved by increasing the number of \mathbb{H} s, but this can lead to overfitting, a high

computational rate, and a slow learning time. The number of groups that are contained within the concealed layers is the second free parameter. There is no overarching principle that can be applied when selecting this parameter. A slower learning time and poorer performance are the inevitable outcomes of having more or fewer units, just as with the numeral of hidden levels. The numeral of tiny batches becomes the third unrestricted parameter. Mini batches have the potential to reduce the amount of computation required by the CDBN network.

3.3. Feature encoding

A feature encoding block is provided with the CDBN features in order to obtain faster performance. This block is responsible for computing more discriminative representations. As a method for encoding features, furthermore make use of the algorithm known as the bag of features [19]. Fig. 4 illustrates the overall structure of the bag of features. First, the codebook that is a collection of code words, is built. The code words represent the CDBN features that have been retrieved. After that, a histogram that displays the occurrence of the code words contained inside the image is used to represent the input image.

A clustering algorithm is utilized in the process of modelling the codebook. In order to determine a collection of centroids in the feature space, each of the retrieved CDBN features is first clustered. Clustering is accomplished with the help of the k means method [20], which is used in this work. The choice of the total number of code words, often known as the size of the codebook, is an essential component in the process of building the codebook. Csurka et al. ([21]) have shown that when it comes to natural image classification, a bigger codebook size yields superior results. Despite this, Tatiana and colleagues ([22]) have shown that the dimensions of the codebook do not have a discernible impact on the precision of the medical picture classification. In order to identify the codebook size that is optimal for the categorization of neuroblastoma histology images, furthermore first examine a variety of codebook sizes and then select the one that performs the best. A histogram of code words is generated to serve as a representation of the input image when the feature encoding block is utilized. Finally, in order to represent the distinct types of neurological tumor histology images, an SVM classifier is trained to categorize the histograms of the information-encoded unit.

Furthermore, utilize the Kyoto natural image dataset [23] to learn the first layer of the CDBN because it has a high number of low-level features, including edges. This is necessary because the first layer of the CDBN is responsible for learning the common visual information, such as edges. The second and third layers receive training with a database consisting of neuroblast tumors. This is done by randomly dividing the database into three subsets: the first one is used for validation and contains 211 photos; the second one is used for training and contains 623 images; and the 3rd one is used for testing and contains 209 images. Using the validation set, furthermore determine the optimal values for the free parameters, and furthermore utilize the training set and the testing set to do the final system evaluation.

3.4. Elephant herd optimization (EHO)

In 2015, Wang et al. presented the EHO algorithm to the scientific community [24]. Elephants engage in social behavior and comprise a complicated hierarchy consisting of females and their young. An elephant group is made up of a number of different clans, each of which is led by a matriarch along with her calves and any other females that are connected to her. A family is founded by a female. EHO is concerned with the hypotheses that come after it. The herd of elephants can be broken down into subgroups known as clans, with particular elephants constituting each clan. There is a certain number of male elephants that break away from their herd to live on their own. There is a matriarch who serves as the leader of each clan. Within the elephant herd, the matriarchal group guards the most effective strategy. Each and every member of the elephant population belongs to one of the j clans. The

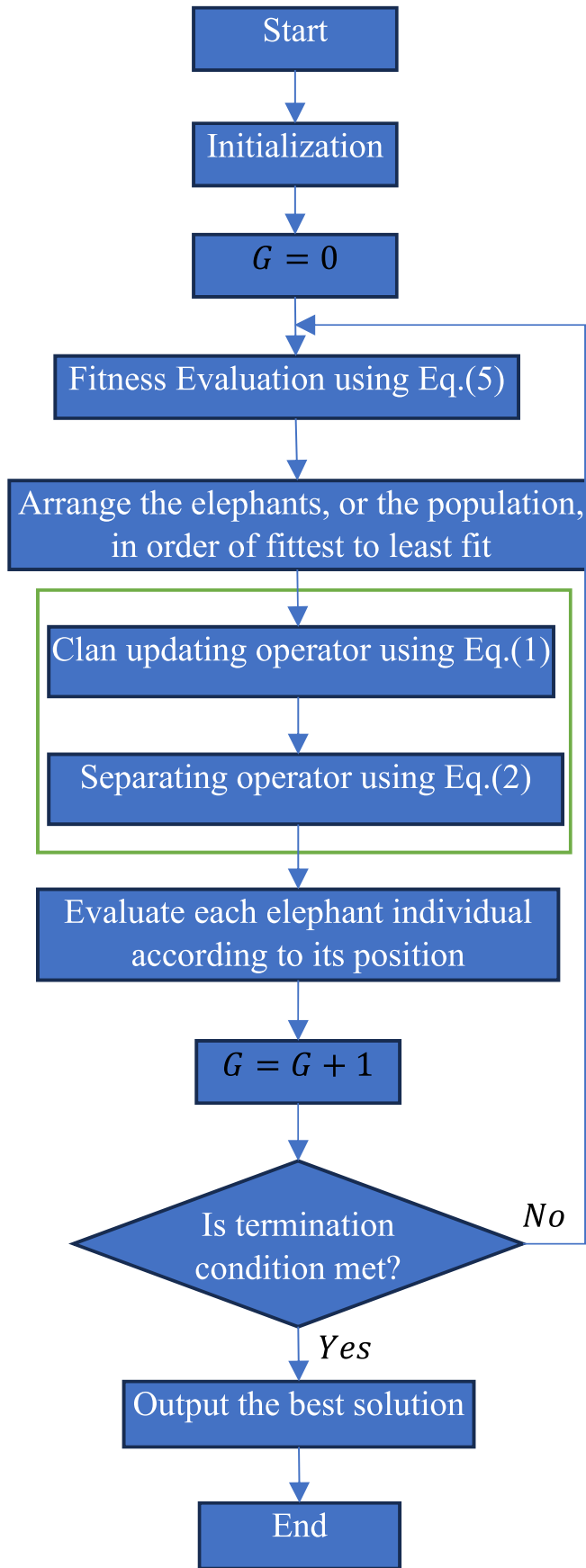


Fig. 5. Flowchart of EHO

new posture of each elephant is influenced by the matriarch, c_i . It is possible to determine the elephant j in clan c_i by utilizing Eq. (1);

$$x_{new, c_i, j} = x_{c_i, j} + \alpha \times (x_{best, c_i} - x_{c_i, j}) \times r \quad (1)$$

where x_{new} , c_i, j denoted the new location and $x_{c_i, j}$ signified the previous location for elephant j within the clan c_i . The matriarch c_i is indicated by the value x_{best, c_i} , which symbolizes the best elephant. The scaling factor, $r \in [0, 1]$, is shown by the expression $\alpha \in [0, 1]$. The most valuable elephant is determined for each clan based on Eq. (2);

$$x_{new, c_i, j} = \beta \times x_{center, c_i, d} \quad (2)$$

In this case, $\beta \in [0, 1]$ denotes the second constraint that directs the influence of the $x_{center, c_i, d}$, which is outlined in the previous sentence.

$$x_{center, c_i, d} = \frac{1}{m_{c_i}} \times \sum_{j=1}^{m_{c_i}} x_{c_i, j, d} \quad (3)$$

Here $1 \leq d \leq D$ and m_{c_i} denote the numeral of elephants in clan $x_{c_i, d}$ represents the d th dimension of individual elephant $x_{c_i, d}$, the center of clan $x_{center, c_i, d}$ can be modified using the equation (eqn. (3)). When trying to find solutions to optimization problems, the process of separating could be modeled as a separation operator. In each clan, the elephants with the lowest value are moved to the position specified in Eq. (4), which is the next available spot.

$$x_{worst, d} = x_{min} + (x_{max} - x_{min} + 1) \times rand \quad (4)$$

In this instance, the bottom and upper bands of the exploration space are denoted by the variables x_{min} and x_{max} , respectively. The random value chosen from a normal distribution is represented by $rand$ when it is in the range $[0, 1]$. The EHO algorithm was evaluated for its performance in a number of standard set functions as well as in medical diagnosis, where it demonstrated improved accuracy. In this particular investigation, the EHO algorithm is utilized for the purpose of DBN parameter optimization. The outcome of the DBN model is based on the weights and the biases of the layers of the network that came before it. In contrast to other optimization techniques, EHO does not use the individuals who came before them in later stages of the updating process. EHO is a swarm-inspired method that deals with global optimization tasks that are considered by clan update and searching actions. EHO is an acronym for Enhanced Hybrid Optimization. Because EHO does not engage in relaxing, it is less susceptible to the effects of noise. They execute better in situations that are limited and optimized for them. Important aspects of EHO include a high convergence rate along with low localization error rates, all while reducing the amount of time needed for execution. The algorithm is capable of directly addressing non-convex ML issues.

3.5. Fine tuning of DBN

In most RBMs, the four fundamental parameters that are adjusted are the learning rate, the momentum weight, the hidden units, and the weight decay. Due to the complexity and divergence of the problem, the use of typical methods to compute the error function is considered an NP-hard task. In order to resolve this issue, metaheuristics have been put to use. In this work, the EHO method is applied in order to perfect the DBN training by adjusting the parameters in minute detail. In this case, the parameters that have been set are as follows: $\eta = [0.1, 0.9]$, $m = [5100]$, $\alpha = [0.00001, 0.01]$, and $\lambda = [0.1, 0.9]$. In order to accomplish what needs to be done, there needs to be a fitness function that directs the search process to the most appropriate responses. The fitness function that is used is referred to as mean squared error (MSE). The equation for this function, which determines the amount of deviation that exists between the actual value and the target value, is provided in (5).

$$\text{MSE} = \frac{1}{T} \sum_{j=1}^N \sum_{i=1}^D (\mathbb{D}_j(i) - \mathbb{Y}_j(i))^2 \quad (5)$$

In most RBMs, the four fundamental parameters that are adjusted are the learning rate, the momentum weight, the hidden units, The EHO searches for a set of DBN parameters that results in the lowest possible MSE value. $\mathbb{D}_j(i)$ symbolizes the value that can be found in the j th unit of the DBN's output layer at the period 't', and $\mathbb{Y}_j(i)$ indicates the j th feature of the chosen value. The procedure is carried out repeatedly up until the point where it can be stopped for good. The following are the steps involved in EHO's optimization process and Fig. 5 show the flowchart of EHO:

1. Initialize the population and set the EHO parameters in the appropriate places.
2. Determine the distinct fitness value of the DBN using the RMSE metric, taking into account both the learning rate and the total numeral of batch learning iterations. Determine the best possible person to use.
3. Determine if the termination condition has been satisfied; if it has, the iteration should be finished, and the result should be produced; otherwise, proceed to the following step.
4. Make necessary adjustments to each individual position. Reset the individuals' values to their default values elsewhere the lower and upper bounds.
5. Begin a novel iteration by modifying the ideal individual using the previous results.

Algorithm 1. optimal parameter selection of DBN by using EHO

```

Algorithm 1: optimal parameter selection of DBN by using EHO
Inputs: the place for elephant j in clan  $c_i$ , the place for elephant j in clan  $c_i$ , appropriate for elephant j in clan  $c_i$   $r \in [0,1]$ , the midpoint of clan  $c_i$ ,  $x_{\max \text{ upper}}$  destined of the elephant place and  $x_{\min \text{ lower}}$  destined of the elephant place  $\text{rand} \in [0,1]$  is a stochastic circulation.
Output: optimal parameter assortment of high fitness rate
Step 1: Beginning. Set generation rate  $t = 1$ ; maximum generation as  $MaxGen$ 
Step 2: While  $< MaxGen$  do
    Category all the elephants bestowing to their fitness.
    For  $c_i = 1$  to  $n$   $c_i$  do
        /Clan apprising operator
        For  $j = 1$  to  $n_{c_i}$  do
            Update  $c_{c_i,j}$  and produce  $x_{\text{new},c_i,j}$  by Eq.(1)
            If  $x_{c_i,j} = x_{\text{best},c_i}$ 
                Then modernized  $x_{c_i,j}$  and produce  $x_{\text{new},c_i,j}$  by Eq.(2)
            End if
        End for  $j$ 
        End for  $c_i$ 
        /Separating operator
        Adjustment the wickedest elephant in clan  $c_i$  by Eq.(4)
    End for  $c_i$  // s
    Measure population by the competent places.
     $t = t + 1$ 
Step 3 End while
Return the results of hyperparameter values.

```

iii. Fully Connected Conditional Random Field Postprocessing

In most RBMs, the four fundamental parameters that are adjusted are the learning rate, the momentum weight, and the hidden units, once predictions were made using the suggested CDBN-EHO technique on

each image patch, furthermore merged the individual tiles back together to form the original image. This stage of stitching can lead to devising the borders of each individual patch, as demonstrated in the last two rows of Fig. 2. In order to solve this issue, the proposed system utilized a Conditional Random Field (CRF) technique in its entirety. Krahenbuhl and Koltun [25] were the first to suggest using this method to efficiently compute picture segmentations. It exhibited the ability to both capture tiny edge information as well as make use of dependencies that are long-range. After that, Chen et al. [26] implemented this strategy into CNNs as an additional processing step so that they could better analyze images. $\mathbb{P}(\mathbb{I}, \mathbb{X}) = \frac{1}{x(\mathbb{I})} \exp(-\mathcal{E}(\mathbb{I}, \mathbb{X}))$ is the formula that describes a CRF (\mathbb{I}, \mathbb{X}) , and it is important to note that \mathbb{X} is defined across the entire picture as $\{\mathbb{x}_1, \mathbb{x}_2, \dots, \mathbb{x}_N\}$ is the total numeral of pixels, and \mathbb{x}_i is the label that corresponds to the pixel that is numbered i . The energy function is incorporated into the technique.

$$\mathcal{E}(\mathbb{I}, \mathbb{X}) = \sum_i \theta_i(\mathbb{x}_i) + \sum_{i,j} \theta_{i,j}(\mathbb{x}_i, \mathbb{x}_{i,j}) \quad (6)$$

where the first term is the unary latent and the 2nd term is the pairwise latent. The unary latent is demarcated as $\theta_i(\mathbb{x}_i) = -\log \mathbb{P}(\mathbb{x}_i)$, where $\mathbb{P}(\mathbb{x}_i)$ is the label obligation probability at pixel i as determined by the segmentation head in the GNH. The unary potential is defined as the difference between these two values. The pairwise potential is defined as the following equation: $\theta_{i,j} = \mu(\mathbb{x}_i, \mathbb{x}_j) \sum_{m=1}^K \omega_m \mathcal{A}^m(\mathbb{f}_i, \mathbb{f}_j)$, where $\mu(\mathbb{x}_i, \mathbb{x}_j) = 1$ if $\mathbb{x}_i \neq \mathbb{x}_j$. Each m represents the Gaussian kernel, which is weighted by a learnable parameter known as m and is dependent on features that have been retrieved from pixels i and j and are designated by the letter f . In the kernels, make use of bilateral position and color terms, following the example given in [46].

$$\omega_1 \exp\left(-\frac{\|\mathbb{p}_i - \mathbb{p}_j\|^2}{2\sigma_\alpha^2}\right) - \frac{\|\mathbb{l}_i - \mathbb{l}_j\|^2}{2\sigma_\beta^2} + \omega_2 \exp\left(-\frac{\|\mathbb{p}_i - \mathbb{p}_j\|}{2\sigma_\gamma^2}\right) \quad (7)$$

where \mathbb{p} stands for the pixel's location and \mathbb{l} for the intensity of the pixel's color. As a result, the first kernel term ensures that neighboring

pixels of a similar color are placed in the same class, whilst the second kernel term gets rid of small patches that are isolated from one another. The “scale” of the Gaussian kernels, which were determined during the trial using an empirical method, is controlled by the hyperparameters σ_α , σ_β and σ_γ , respectively. In the subsequent parts of this study, for the sake of convenience, furthermore will refer to fully linked CRF as CRF.

4. Experimental results and discussion

In this part, furthermore will provide a quick overview of the proposed CDBN-EHO experiment design, then present a number of experimental data to validate the suggested design for the epithelial cell identification and Gleason grading operations. The consequences of the technique’s instance segmentation were translated into the semantic segmentation outcomes by selecting the instance class with the highest probability at each pixel location. This was done so that the new findings could be easily compared to the work that had been done previously. The suggested method is analyzed, and its performance is compared to that of the already established routes R-CNN [27], CNN [9], and DNN [8]. This section employs the conventional metrics: OPA (Overall Pixel Accuracy), Standard Mean Accuracy (SMA), mean Intersection Over Union (mIOU), in addition recall, accuracy, precision, and F-measure

are used to evaluate the performance of segmentation findings. This allows us to make This suggested technique comparable with earlier work. The following is an explanation of how these metrics are defined. Assume that furthermore have the results of the segmentation known as sf , the ground truth label known as tl , and a pixel-wise confusion matrix known as Cm . Here, Cm_{ij} represents the number of pixels that were labeled as tl_i and were predicted to be sf_j . The mIOU is defined as the mean of all of the individual Jaccard coefficients, which are denoted by the notation J_i , for each class tl_i . Here makes use of the definition of the Jaccard index in order to derive J_i from the confusion matrix Cm .

$$J_i = \frac{\text{TruePositive}}{\text{TruePositive} + \text{False Positive} + \text{False Negative}} = \frac{Cm_{i,i}}{tp_i + P_i - Cm_{i,i}} \quad (8)$$

where $tp_i = \sum_{j=1}^N Cm_{i,j}$ denotes the total numeral of pixels with label tl_i . $P_j = \sum_i Cm_{i,j}$ denotes the number of pixels predicted as fj . The mIOU is then specified by

$$J = \frac{1}{N} \sum_i^N J_i \quad (9)$$

where N is the number of classes. The OPA is defined as

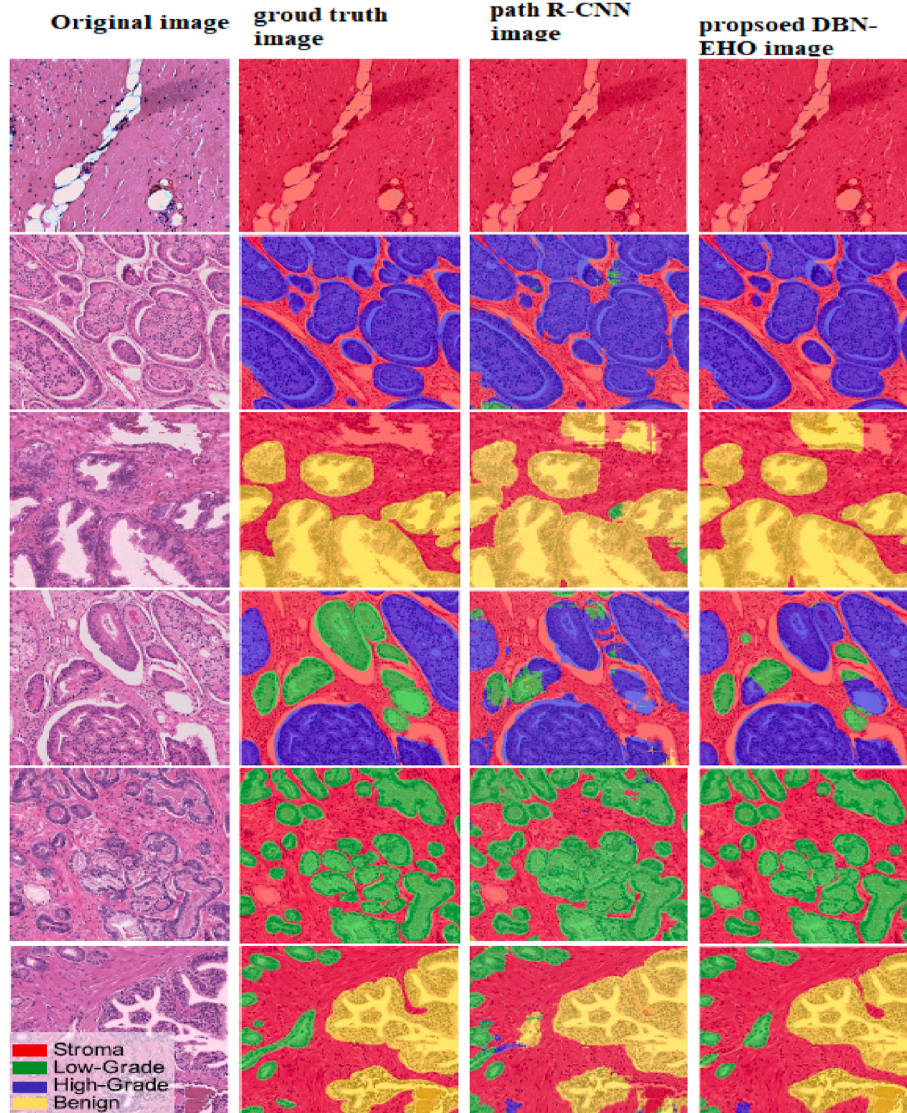


Fig. 6. Proposed CDBN-EHO technique results among existing technique.

$$OPA = \frac{\sum_i Cm_{ii}}{\sum_i \sum_j Cm_{ij}} \quad (10)$$

The SMA is well-defined as

$$SMA = \frac{1}{N} \sum_i \frac{Cm_{ii}}{\sum_j Cm_{ij}} \quad (11)$$

For the purpose of extracting features from the input pathological image, this section made use of a ResNet [28] in the suggested CDBN-EHO technique. Both the RPN and the GNH make use of a structure known as a feature pyramid network (FPN) [29], which involves the substitution of feature pyramids for single-scale feature maps. The FPN creates feature pyramids with the format $\{P_2, \dots, P_6\}$, as described in Ref. [29]. At each individual feature pyramid, here placed a unique scale anchor that corresponds to a potential region of interest for the RPN. After that, the RPN is trained with the parameters that are shared across all levels of the feature pyramid. Furthermore allocate each Region of Interest (ROI) on the input picture to the GNH network, which has dimensions of width w_i and height ht , to the feature pyramid Py_k using the following formula:

$$Py_k = \left\lfloor k_0 + \log_2 \left(\sqrt{w_i * ht / 224} \right) \right\rfloor \quad (12)$$

If the scale of the ROI is reduced (for example, to 1/2 of 224), the equation eqn. (12) suggests that the data should be mapped onto a level with a higher resolution (for example, $k = 3$). The information that the technique needs to send into the GNH is extracted from each ROI by the technique using this technique, which is done on a similar scale. The outcomes of the projected and existing technique are illustrated in Fig. 6. The suggested technique yields mIOU scores of 81.32 %, SMA scores of 89.78 %, and OPA scores of 90.40 % across all four classes. Path R-CNN has a performance that is considered to be above average in the

“stroma”, “benign”, and “high-grade” classifications, among these four categories. In spite of this, it only receives a “low-grade” IOU score of 71.54 %. This is because “low-grade” glands can have a wide range of appearances from one another. The glands that are “lowgrade” might vary in size and shape, although they are typically long and/or angular in shape. The majority of them are microglandular, however some of them might be anywhere from medium to enormous in size. This diversity in size and shape is very clear in the second column of Fig. 6, where “low-grade” glands are represented by the green hue. This variance can be plainly observed.

Fig. 7 depicts the results obtained by the suggested technique after the ENH and CRF were included. It demonstrates that the ENH provides a significant improvement to the performance of the segmentation. This is primarily due to the fact that This technique settings need us to make a choice between the accuracy of This objectless prediction and the accuracy of This segmentation. If Furthermore want This system to have a high accuracy that minimizes the failure to detect possible epithelial regions, then Furthermore need to lower the detection threshold when ENH is not present because that will allow us to have high precision. This will provide us with a technique that is meant to forecast epithelial cells

Table 2

Overall performance evaluation among all cancer segmentation schemes.

Performance metrics (%)	Proposed CDBN-EHO	Path R-CNN	CNN	DNN
Accuracy	95.86	94.75	92.64	93.41
Precision	97.32	96.67	94.22	92.60
Recall	97.88	96.77	95.19	94.57
F-measure	97.95	96.77	95.19	94.08
mIOU	81.32	77.56	74.22	72.60
SMA	89.78	87.58	83.53	82.43
OPA	90.40	88.9	87.6	84.08

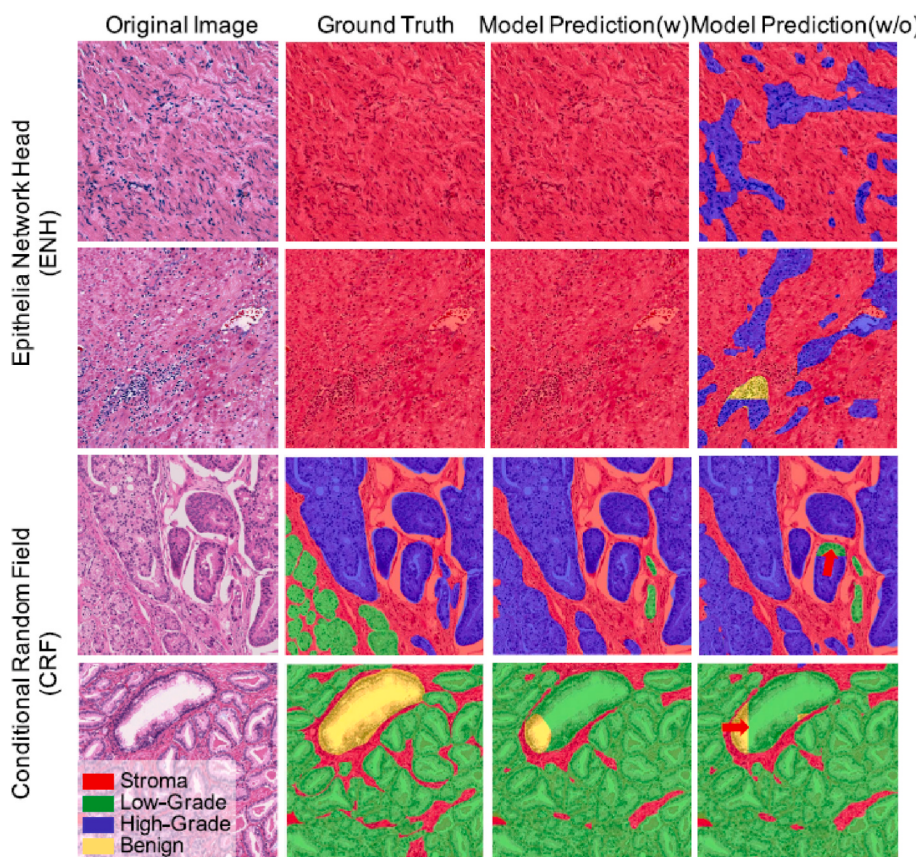


Fig. 7. The effectiveness of incorporating the ENH and CRF into the proposed CDBN-EHO structure.

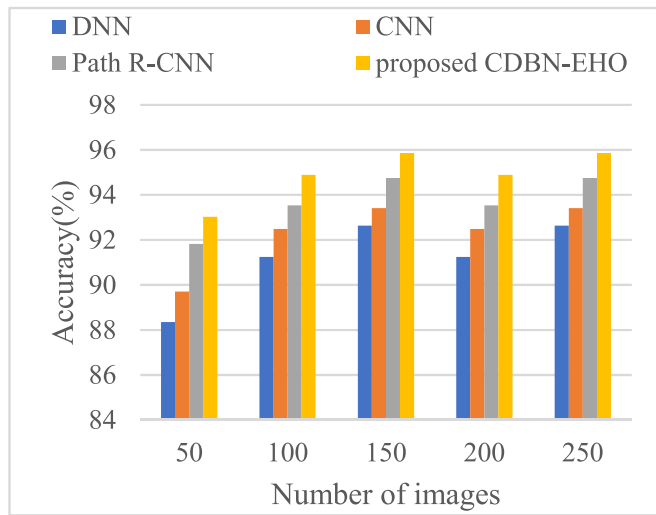


Fig. 8. PC segmentation accuracy prediction among methods.

more frequently even in an image that is full of stroma; as a result, the performance will be drastically lowered. The first two rows of Fig. 7 are a good example of this phenomenon. Furthermore, can observe that the technique has a tendency to anticipate ROIs in vast sections of stroma by looking at the very last column. As a result, the proposed technique arrives at the conclusion that the ENH is essential to the success of achieving good performance in the proposed system. In the Supplementary Information, further justifications and benefits of the ENH are explored. As can be seen in the last two rows of Fig. 5, the results that have been proposed utilizing the CRF reveal that the addition of the approach helps remove the unnatural borders that are caused by stitching. The unnatural boundaries that were produced as a result of the stitching procedure are denoted by the red arrows in the picture (Rows 3 and 4). After the CRF has been post-processed, furthermore see that these artificial borders have been erased. Additionally, the CRF contributes to a moderate improvement in mIOU.

The total performance of the proposed CDBN-EHO in comparison to other current systems such as R-CNN, CNN, and DNN is displayed in Table 2. It is concluded that the suggested CDBN-EHO achieved great performance results in comparison to existing schemes due to their capacity to process huge datasets and need less computational time. The performance of DBN has been boosted across the board thanks to the

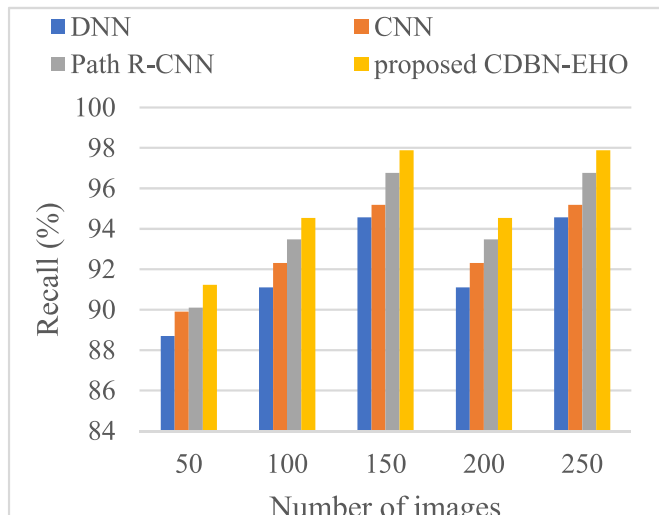


Fig. 10. PC segmentation recall prediction among methods.

careful optimization of its parameters.

Fig. 8 depicts the accuracy of PC segmentation achieved by the proposed CDBN-EHO algorithm and evaluates its performance in comparison to that of other current segmentation methods such as route R-CNN, CNN, and DNN. Due to a reduction in the amount of computing time required, the accuracy of the projected technique improved along with the number of photos that were used. Based on the findings, it can be deduced that the proposed CDBN-EHO algorithm yields high accuracy results of 95.86 %, whereas the accuracy yielded by other classifiers, such as R-CNN, CNN, and DNN, respectively, is 94.75 %, 92.64 %, and 93.41 %. The performance of DBN has improved as a result of the optimal prediction of parameter value.

Fig. 9 displays the precision of PC segmentation achieved by the proposed CDBN-EHO algorithm, which was tested in comparison to other current segmentation schemes such as route R-CNN, CNN, and DNN. Due to a reduction in the amount of computing time required, the precision of the proposed strategy improved along with the number of photos that were used. Based on the findings, it can be deduced that the suggested CDBN-EHO algorithm achieves high precision results of 97.32 %, but other classifiers, such as the R-CNN, CNN, and DNN techniques, only achieve precision values of 96.67 %, 94.22 %, and 92.60 % values respectively. The study comes to the conclusion that the

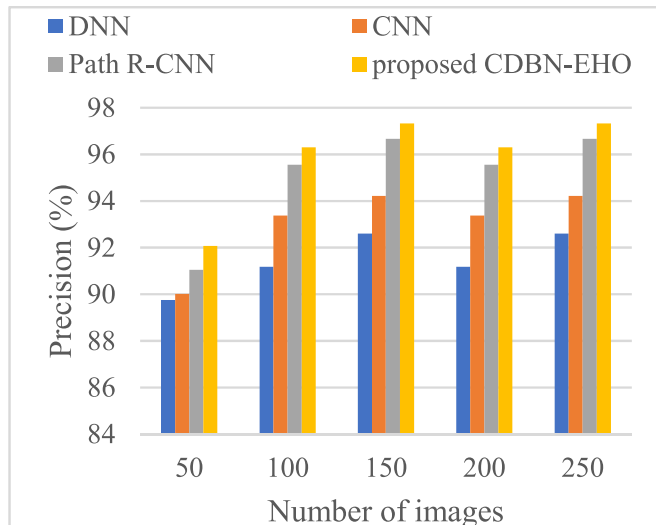


Fig. 9. PC segmentation precision prediction among methods.

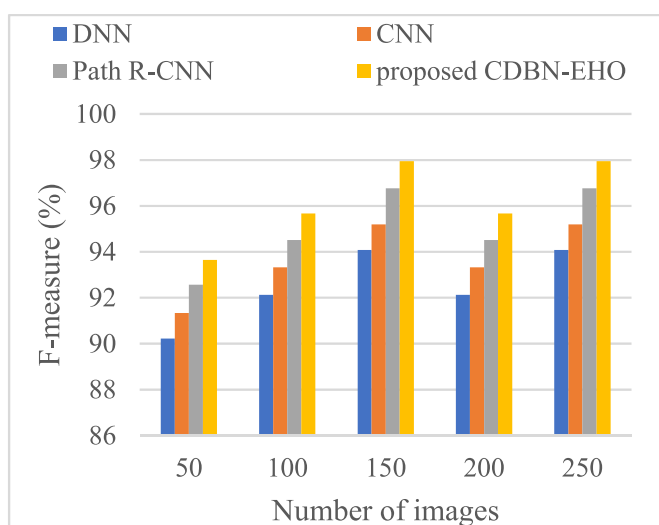


Fig. 11. PC segmentation F-measure prediction among methods.

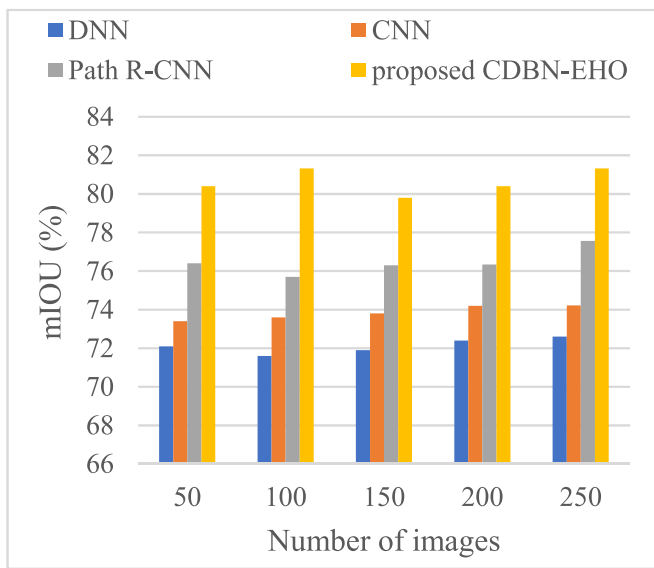


Fig. 12. PC segmentation mIoU prediction among methods.

CDBN-EHO research method performs better when compared to other methodologies.

The PC segmentation recall of the proposed CDBN-EHO is displayed in Fig. 10, and it is evaluated in comparison to other existing segmentation methods such as route R-CNN, CNN, and DNN. Due to a reduction in the amount of computing time required, the recall of the suggested technique improved along with the number of photos that were used. Based on the findings, it can be deduced that the suggested CDBN-EHO method achieves high recall results of 97.88 %, but other classifiers, such as the R-CNN, CNN, and DNN techniques, only achieve recall values of 96.77 %, 95.19 %, and 94.57 % values respectively. The study comes to the conclusion that the CDBN-EHO research method performs better when compared to other methodologies.

The PC segmentation F-measure of the proposed CDBN-EHO is displayed in Fig. 11, and it is evaluated in comparison to other current segmentation schemes such as path R-CNN, CNN, and DNN. Due to the decreased amount of time spent computing, the F-measure of the suggested scheme increased along with the number of images as they were added. Based on the findings, one may draw the conclusion that the

suggested CDBN-EHO algorithm achieves high F-measure results of 97.95 %, whereas other classifiers, such as R-CNN, CNN, and DNN techniques, generate F-measure values of 96.77 %, 95.19 %, and 94.08 % values respectively. It comes to the conclusion that research work is more successful when paired up with other methods.

Fig. 12 depicts the PC segmentation mIoU of the proposed CDBN-EHO, which was then evaluated in comparison to other current segmentation schemes such as route R-CNN, CNN, and DNN. Because there is less time spent computing, the mIoU of the proposed approach increases in proportion to the number of photos that are being used. Based on the findings, it can be deduced that the proposed CDBN-EHO algorithm achieves high mIoU results of 81.32 %, whereas other classifiers, such as R-CNN, CNN, and DNN techniques, only achieve mIoU values of 77.56 %, 74.22 %, and 72.60 %, respectively. The study comes to the conclusion that the CDBN-EHO research method performs better when compared to other methodologies.

Fig. 13 depicts the PC segmentation SMA of the proposed CDBN-EHO, which was then evaluated in comparison to other current segmentation methods such as route R-CNN, CNN, and DNN. Due to the reduced amount of time spent computing, the SMA of the suggested approach increases together with the number of photos that are being used. Based on the findings, it can be deduced that the proposed CDBN-EHO algorithm achieves high SMA results of 89.78 %, while other classifiers, such as R-CNN, CNN, and DNN techniques, only achieve SMA values of 87.58 %, 83.53 %, and 82.43 % respectively. The study comes to the conclusion that the CDBN-EHO research method performs better when compared to other methodologies. The proposed method achieves high SMA through a combination of innovative methodologies, effective Bayesian inference, multi-task learning, optimized parameterization, and comprehensive evaluation. By introducing novel optimization techniques like EHO-based Hyper-parameter CDBN and grading network head-optimized DBN, the model effectively captures relevant features and contextual information crucial for accurate histological image analysis. Leveraging an extremely effective Bayesian inference approach for fully linked CRF techniques ensures precise segmentation, contributing to the overall accuracy of the model. The multi-task approach enables simultaneous consideration of multiple tasks, enhancing performance by leveraging shared contextual information across tasks. Additionally, optimized parameterization minimizes overfitting and algorithmic sensitivity, ensuring robust performance across diverse datasets and clinical scenarios. This comprehensive evaluation using SMA reflects the model's reliability and effectiveness in

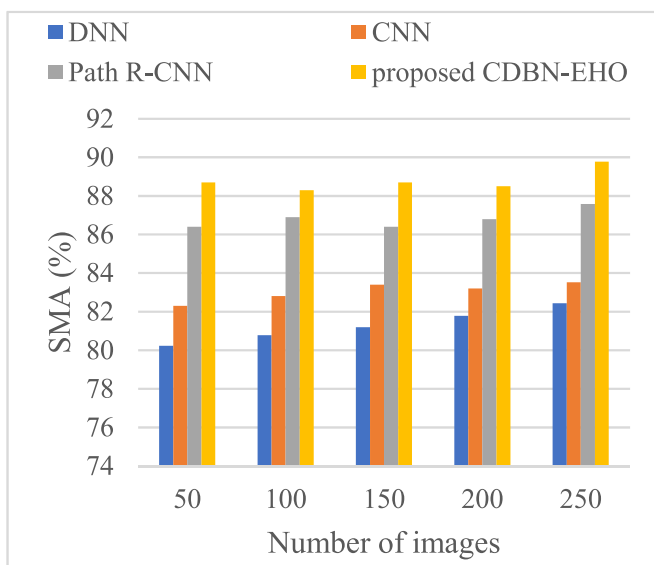


Fig. 13. PC segmentation SMA prediction among methods.

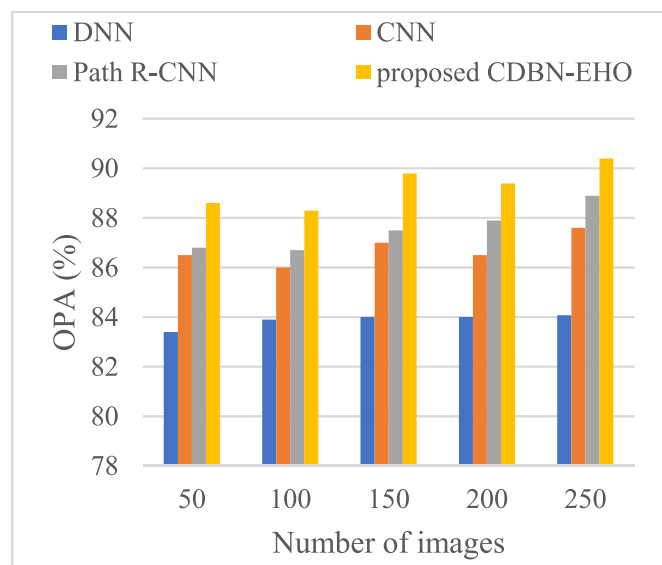


Fig. 14. PC segmentation OPA prediction among methods.

real-world clinical settings, particularly in tasks like prostate cancer diagnosis and Gleason grading.

Fig. 14 depicts the PC segmentation OPA of the proposed CDBN-EHO, which was then evaluated in comparison to other existing segmentation methods such as route R-CNN, CNN, and DNN. The OPA of the proposed technique grew when there was less time spent computing, which led to an increase when the number of photos was increased. Based on the findings, it can be deduced that the suggested CDBN-EHO algorithm achieves high OPA results of 90.40 %, whereas other classifiers, such as R-CNN, CNN, and DNN algorithms, generate OPA values of 88.9 %, 87.6 %, and 84.08 % values respectively. It comes to the conclusion that research work is more successful when paired up with other methods. The high OPA achieved by the proposed method can be attributed to several key factors. The model effectively delineates boundaries and structures within histological images through precise segmentation techniques. By accurately identifying pixel-level details, the model ensures that each pixel is correctly classified, leading to high pixel accuracy. The proposed method utilizes advanced DL architectures, such as CDBNs, which are optimized for pixel-level classification tasks. The architecture is designed to capture intricate patterns and features within the images, contributing to accurate pixel-wise predictions. The evaluation of OPA provides a comprehensive assessment of the model's performance at the pixel level, accounting for both true positive and true negative predictions. This holistic evaluation metric ensures that the model's segmentation results are accurate and reliable, further validating its effectiveness in histological image analysis tasks.

5. Conclusion

In conclusion, our paper introduces the innovative CDBN-EHO framework alongside a grading network head-optimized deep belief network technique for multi-task prediction in histological image analysis. We leverage advanced methodologies such as Bayesian inference for segmentation using fully linked Conditional Random Field techniques, with pairwise boundary capacities determined by a linear mixture of Gaussian kernels. Our approach demonstrates the potential to enhance performance by incorporating more contextual information through multi-task learning. Overall, this research contributes to advancing histological image analysis and lays the groundwork for the development of more accurate, efficient, and interpretable diagnostic tools for improving patient care in domains such as cancer diagnosis and treatment. This was the case in terms of accuracy, precision, recall, f-measure, 88.78 % SMA, 79.56 % mIOU, and 89.40 % OPA, to name a few metrics. In the future, the identification of PC systems will be improved by employing the feature selection and ranking phase with various hybrid optimization methods. This will be done in order to improve accuracy. In addition, granular computing will be included into DNNs in the near future in order to greatly rise the pace of calculation. Moving forward, several avenues of future work are identified. Firstly, we aim to further optimize our framework to mitigate algorithmic sensitivities and enhance generalization across diverse datasets and clinical scenarios. Additionally, efforts will be directed towards improving the interpretability of our models to foster greater trust among clinicians. The computational complexity and trade-offs of different methods for histopathological image analysis in prostate cancer diagnosis are crucial considerations. Techniques like the Elephant Herding Optimization-based Hyper-parameter Convolutional Deep Belief Network (CDBN-EHO) may offer breakthrough results but could potentially require more memory space and time compared to other methods like R-CNN, CNN, and DNN. Evaluating these trade-offs is essential for selecting the most suitable approach for accurate and timely diagnosis, considering the urgency of detecting and treating prostate cancer, the second highest cause of cancer-related deaths in men globally.

CRediT authorship contribution statement

S. Angel Latha Mary: Investigation, Methodology, Project administration. **S. Siva Subramanian:** Conceptualization, Data curation, Formal analysis. **G. Priyanka:** Validation, Visualization. **T. Vijayakumar:** Writing – original draft, Writing – review & editing. **Suganthi Alagumalai:** Resources, Software, Supervision.

Declaration of competing interest

The authors declare the following financial interests/personal relationships which may be considered as potential competing interests: Suganthi Alagumalai is currently employed by JPMorgan Chase, where she serves as an Agility Lead role within the Cyber Security division.

References

- [1] PC: The Leading Cancer in India.
- [2] S. Ghai, M.A. Haider, Multiparametric-MRI in diagnosis of PC, *Indian J. Urol: j. Urol. Soc. India* 31 (3) (2015) 194.
- [3] R. Loffroy, O. Chevallier, M. Moulin, S. Favelier, P.Y. Genson, P. Pottecher, L. Cormier, Current role of multiparametric magnetic resonance imaging for PC, *Quant. Imag. Med. Surg.* 5 (5) (2015) 754.
- [4] Rights, P. B. O., Chipko, C. R., Judy, G. D., Liebman, L. R., Pennington, J. D., Siddiqui, O., ... & Links, R. O. A. Radiation Therapy for PC.
- [5] D.A. Barron, D.R. Rowley, The reactive stroma microenvironment and PC progression, *Endocr. Relat. Cancer* 19 (6) (2012) R187–R204.
- [6] S. Iqbal, G.F. Siddiqui, A. Rehman, L. Hussain, T. Saba, U. Tariq, A.A. Abbasi, PC detection using DL and traditional techniques, *IEEE Access* 9 (2021) 27085–27100.
- [7] 1. Saqib Iqbal, Ghazanfar Farooq Siddiqui, Amjad Rehman, Lal Hussain, Tanzila Saba, Usman Tariq, Adeel Ahmed Abbasi, PC detection using DL and traditional techniques *IEEE Access* 9 (2021) 27085–27100.
- [8] Yuchun Li, Mengxing Huang, Yu Zhang, Jing Chen, Haixia Xu, Gang Wang, Wenlong Feng, Automated gleason grading and gleason pattern region segmentation based on DL for pathological images of PC, *IEEE Access* 8 (2020) 117714–117725.
- [9] Davood Karimi, Guy Nir, Ladan Fazli, Peter C. Black, Larry Goldenberg, Septimiu E. Salcudean, DL-based gleason grading of PC from histopathology images—role of multiscale decision aggregation and data augmentation, *IEEE J. Biomed Health Inf.* 24 (5) (2019) 1413–1426.
- [10] Lourdes Duran-Lopez, Juan P. Dominguez-Morales, Antonio Felix Conde-Martín, Saturnino Vicente-Díaz, Alejandro Linares-Barranco, PROMETEO: a CNN-based computer-aided diagnosis system for WSI PC detection, *IEEE Access* 8 (2020) 128613–128628.
- [11] Ohad Kott, Drew Linsley, Ali Amin, Andreas Karagounis, Carleen Jeffers, Dragan Goljanian, Thomas Serre, Boris Gershman, Development of a DL algorithm for the histopathologic diagnosis and Gleason grading of PC biopsies: a pilot study, *Eur. Urol. focus* 7 (2) (2021) 347–351.
- [12] Dallin Busby, Ralph Grauer, Krunal Pandav, Akshita Khosla, Parag Jain, Mani Menon, G. Kenneth Haines III, Carlos Cordon-Cardo, Michael A. Gorin, Ashutosh K. Tewari, Applications of artificial intelligence in PC histopathology, in: *Urologic Oncology: Seminars and Original Investigations*, Elsevier, 2023.
- [13] Misbah Ahmad, Imran Ahmed, Ahmed Ouameur Messaoud, Gwanggil Jeon, Classification and detection of cancer in histopathologic scans of lymph node sections using convolutional neural network, *Neural Process. Lett.* (2022) 1–16.
- [14] Zaneta Swiderska-Chadaj, Thomas de Bel, Lionel Blanchet, Alexi Baidoshvili, Dirk Vossen, Jeroen van der Laak, Geert Litjens, Impact of rescanning and normalization on convolutional neural network performance in multi-center, whole-slide classification of PC, *Sci. Rep.* 10 (1) (2020) 14398.
- [15] Abhinav Kumar, Sanjay Kumar Singh, K. Lakshmanan, Sonal Saxena, Sameer Shrivastava, A novel cloud-assisted secure deep feature classification framework for cancer histopathology images, *ACM Trans. Internet Technol.* 21 (2) (2021) 1–22.
- [16] Andrea Chatrian, Korsuk Sirinukunwattana, Clare Verrill, Jens Rittscher, Towards the identification of histology-based subtypes in PC, in: 2019 IEEE 16th International Symposium on Biomedical Imaging (ISBI 2019), IEEE, 2019, pp. 948–952.
- [17] N. Ing, et al., Semantic segmentation for PC grading by convolutional neural networks, *Proc. SPIE* 10581 (Mar. 2018) 105811B.
- [18] A. Gertych, et al., Machine learning approaches to analyze histological images of tissues from radical prostatectomies, *Comput. Med. Imag. Graph.* 46 (Dec. 2015) 197–208.
- [19] Stephen O'Hara, Bruce A. Draper, Introduction to the Bag of Features Paradigm for Image Classification and Retrieval, 2011 arXiv preprint arXiv:1101.3354.
- [20] Tapas Kanungo, David M. Mount, Nathan S. Netanyahu, Christine D. Piatko, Ruth Silverman, Angela Y. Wu, An efficient k-means clustering algorithm: analysis and implementation, *IEEE Trans. Pattern Anal. Mach. Intell.* 24 (7) (2002) 881–892.
- [21] G. Csurka, C.R. Dance, L. Fan, J. Willamowski, C. Bray, Visual categorization with bags of keypoints, in: *Workshop on Statistical Learning in Computer Vision*, 2004, pp. 1–22.

- [22] T. Tatiana, O. Francesco, C. Barbara, CLEF2007 image annotation task: an SVM-based cue integration approach, in: Proceedings of Image CLEF, 2007.
- [23] H. Lee, Y. Largman, P. Pham, H. Lee, P. Pham, Y. Largman, Unsupervised feature learning for audio classification using convolutional deep belief networks, in: 22nd International Conference on Neural Information Processing Systems, ACM, Vancouver, British Columbia, Canada, 2009, pp. 1096–1104.
- [24] M. Nayak, S. Das, U. Bhanja, M.R. Senapati, Elephant herding optimization technique based neural network for cancer prediction, *Inform. Med. Unlocked* 21 (2020) 100445.
- [25] P. Krähenbühl, V. Koltun, Efficient inference in fully connected CRFs with Gaussian edge potentials, in: Proc. Adv. Neural Inf. Process. Syst., 2011, pp. 109–117.
- [26] L.-C. Chen, G. Papandreou, I. Kokkinos, K. Murphy, A.L. Yuille, DeepLab: semantic image segmentation with deep convolutional nets, atrous convolution, and fully connected CRFs, *IEEE Trans. Pattern Anal. Mach. Intell.* 40 (4) (Apr. 2017) 834–848.
- [27] W. Li, J. Li, K.V. Sarma, K.C. Ho, S. Shen, B.S. Knudsen, C.W. Arnold, Path R-CNN for PC diagnosis and gleason grading of histological images, *IEEE Trans. Med. Imag.* 38 (4) (2018) 945–954.
- [28] K. He, X. Zhang, S. Ren, J. Sun, Deep residual learning for image recognition, in: Proc. IEEE Conf. Comput. Vis. Pattern Recognit., Jun. 2016, pp. 770–778.
- [29] T.-Y. Lin, P. Dollár, R. Girshick, K. He, B. Hariharan, S.J. Belongie, Feature pyramid networks for object detection, *Proc. CVPR* 1 (2) (Jul. 2017) 4.